# Effects of Halothane on Dipalmitoylphosphatidylcholine Liposomes: A Raman Spectroscopic Study

Norman C. Craig,*,‡ Gail J. Bryant,§ and Ira W. Levin*

*Laboratory of Chemical Physics, National Institute of Diabetes and Digestive and Kidney Diseases, National Institutes of Health, Bethesda, Maryland 20892*

*Received August 4, 1986; Revised Manuscript Received December 23, 1986*

ABSTRACT: Raman spectroscopy has been used to monitor the concentration of halothane (1-bromo-1-chloro-2,2,2-trifluoroethane) in 20% aqueous dispersions of dipalmitoylphosphatidylcholine (DPPC) as well as to follow changes in the acyl chain order within the hydrocarbon interior of the liposomes. Temperature profiles for the gel to liquid-crystalline phase transitions for the liposomes were constructed from changes in peak height intensity ratios in the C–H stretching mode and C–C stretching mode regions. Halothane present at the clinical level produces a change of −0.5 °C in the phase transition temperature. A limiting transition temperature of about 21 °C and saturation of the gel phase occur when the molar ratio of halothane to DPPC reaches about 1.25. At molar ratios above 2.1, the liquid-crystalline phase is also saturated with halothane. Calculations of the distribution of halothane between the various phases in the system are presented and used to interpret literature data as well as the present experiments. Ideal solution theory accounts rather well for the depression in the transition temperature over most of the mole ratio range, an outcome which implies that halothane is excluded from the hydrocarbon interior but not the head-group region in the gel phase. The role of halothane in the head-group region is discussed.

Although the exact sites and mechanism of general anesthetic action resist definition, current views usually attribute the phenomenon to effects of phospholipid-mediated perturbations on protein function in excitable membranes [see, for example, Ueda and Kamaya (1984), Janoff and Miller (1981), and Roth (1979)]. Since there are numerous theories relating the molecular consequences of solubility in lipids to anesthetic potency (Janoff & Miller, 1981), much effort has been directed recently toward investigating the interactions specifically of the class of inhalation anesthetics with both model and intact membrane assemblies. Unfortunately, manipulation of these gaseous agents, in contrast to nonvolatile anesthetics (O'Leary et al., 1984), often leads to difficulties and ambiguities in adequately describing the partitioning behavior of the inhalation anesthetic between the various phases of the membrane dispersion (Lieb et al., 1981; Janoff et al., 1981; Simon et al., 1979; Mountcastle et al., 1978; Rosenberg et al., 1975; Koehler et al., 1977). The purpose of the present study is to apply vibrational Raman spectroscopy together with a detailed analysis of the partition coefficients of halothane toward clarifying the bilayer perturbations arising from the introduction of an inhalation anesthetic.

Among the variety of physical techniques available for monitoring and assessing the molecular order within a lipid bilayer matrix, Raman spectroscopy provides a sensitive means for investigating the structural and dynamic details accompanying molecular reorganization in multilamellar liposomal dispersions (Levin, 1984; Wong, 1984). In this study, we examine the Raman spectra reflecting both halothane itself and the acyl chain region of the dipalmitoylphosphatidylcholine (DPPC)[1] bilayers to determine directly halothane concentrations throughout the dispersion and to describe the effect of various concentrations of the anesthetic perturbant on the gel to liquid-crystalline phase transition behavior of the DPPC liposomes. Since at low halothane/DPPC mole ratios halothane partitions between the air, water, and phospholipid phases of the dispersion, we use the available literature data to calculate in detail the distribution of the anesthetic in the bilayer environment. The halothane distribution expressions are used specifically to characterize the response of the bilayer dispersions to clinical concentrations of the anesthetic. Indirect evidence from the partitioning behavior of halothane is used to infer the location of the anesthetic agent within the DPPC bilayer in both its gel and its liquid-crystalline forms.

## Experimental Procedures

Halothane (Hal; 1-bromo-1-chloro-2,2,2-trifluoroethane; $M_r$ 197.4) was obtained from Halocarbon Laboratories, Hackensack, NJ, and used as supplied commercially for early experiments. Material which had been distilled away (bp 50 °C) from the 0.01% thymol preservative was used in subsequent experiments. High-purity (99%) synthetic 1,2-dipalmitoyl-DL-phosphatidylcholine (anhydrous, $M_r$ 734.1, density 0.80 g/mL) and *n*-hexadecane (99% purity) were obtained from Sigma Chemical Co. and Supelco, Inc., respectively. These materials were used without further purification.

DPPC multilamellar dispersions in distilled water (20% w/w) were prepared by vortex mixing for approximately 20 min while maintaining the mixture at a temperature above the 41 °C lipid gel to liquid-crystalline phase transition temperature. Halothane–phospholipid dispersion mixtures for the Raman experiments were prepared in Kimax melting point capillaries of 1.5–1.8-mm diameter. To aid the mixing process, a piece of 304 stainless-steel wire (0.7 cm long × 0.8-mm diameter) was included in each sample tube after sample 5. After a measured volume of halothane was injected from a 1- or 5-μL Hamilton syringe under the surface of a weighed

‡ Permanent address: Department of Chemistry, Oberlin College, Oberlin, OH 44074.

§ Present address: Division of Cancer Biology and Diagnosis, National Cancer Institute, National Institutes of Health, Bethesda, MD 20892.

[1] Abbreviations: DMPC, dimyristoylphosphatidylcholine; DPPC, dipalmitoylphosphatidylcholine; Gel, gel state; Hal, halothane (1-bromo-1-chloro-2,2,2-trifluoroethane); LC, liquid-crystalline state.

This article not subject to U.S. Copyright. Published 1987 by the American Chemical Society

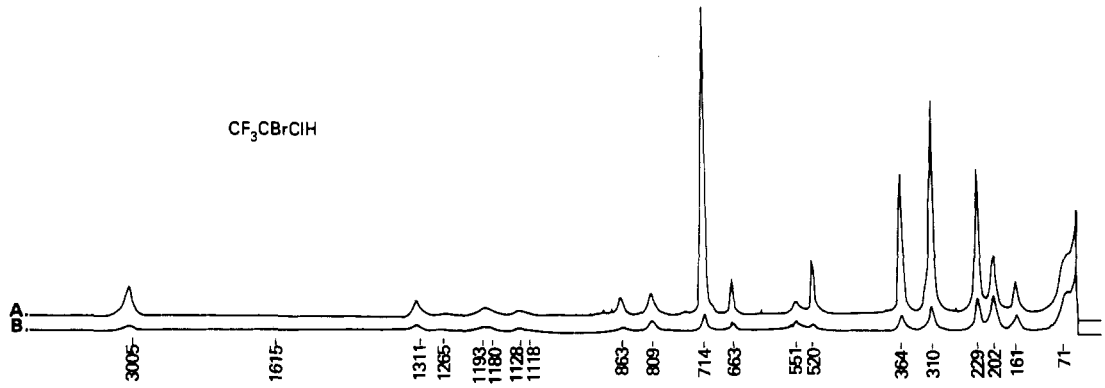


FIGURE 1: Raman spectrum of neat halothane with the polarization analyzer set parallel (upper trace) and perpendicular (lower trace) to the laser beam.

portion (about 45 mg) of the dispersion in a sample capillary, the tube was flame sealed, and both parts were reweighed. The enclosed air volume was about equal to that of the dispersion. From the weighings, which were performed on a semimicro balance, the molar ratios of halothane to phospholipid ($n_{Hal}/n_{DPPC}$) were computed. Samples were incubated above 45 °C for 1 h and mixed from time to time with the aid of a small magnet. For $n_{Hal}/n_{DPPC}$ below 2.1, a uniform, though turbid, mixture was formed after dispersal of the visible halothane bubble. At higher molar ratios, a separate halothane phase remained despite continued mixing. Finally, the multilayer dispersions in the capillary were compacted in a hematocrit centrifuge. For samples 2–5, repeated sequences of inversion and centrifugation of the capillary were used to promote mixing. Solutions of halothane in hexadecane were prepared by weight in Kimax capillaries but were sealed with Parafilm. Neat halothane was handled in the same manner.

For Raman spectroscopy, the capillary sample tubes were inserted into a horizontal hole in a thermostated brass block. To improve thermal contact, the two ends of the sample tube were prewrapped tightly with aluminum foil. The mid portion of the block was cut away in order to permit excitation by the laser through a small orifice and observation of the scattered light from a larger window. The laser radiation was incident on a portion of the sample that contained compacted phospholipid multilayers but not the stainless-steel mixing wire. Temperatures, monitored by a copper–constantan thermocouple embedded in the block, were controlled to ±0.05 °C.

Raman spectra were recorded with a Spex Ramalog 6 spectrometer equipped with plane holographic gratings. The excitation source was a Coherent CR-3 argon ion laser which supplied about 135 mW of 514.5-nm light at the sample. The spectral resolution was about 5 $cm^{-1}$. The instrument was calibrated with atomic argon lines (Craig & Levin, 1980), and reported frequencies are accurate to ±2 $cm^{-1}$. Spectra were acquired at a scan rate of 1 $cm^{-1}/s$ with the aid of Nicolet 1180 computer system. Using signal accumulation techniques, we obtained satisfactory spectra for the 2800–3100-, 990–1200-, and 250–460-$cm^{-1}$ regions with less than 5, 15, and 20 scans per region, respectively. Peak height intensity ratios were calculated from unsmoothed spectra and used to construct temperature profiles. In recording the spectrum of neat halothane, at a scan rate of 2 $cm^{-1}/s$, a polarization analyzer was placed in the collection optics. For all other experiments, the polarization analyzer was not used.

## RESULTS

*Raman Spectrum of Halothane.* The characteristics of the Raman spectrum of halothane allow a direct determination of the concentration of halothane in aqueous phospholipid dispersions over a wide range of composition. Figure 1 shows the Raman spectrum of neat liquid halothane recorded with the two standard $I_{\parallel}$ and $I_{\perp}$ settings of the polarization analyzer. The overall spectrum is in good agreement with the random polarization spectrum recorded photographically by Thiemer and Nielsen (1957) with 435.8-nm mercury arc excitation. The frequencies of the halothane bands are almost unchanged by dissolution in a hydrocarbon solvent. With the exception of a 3-$cm^{-1}$ decrease of the C–H stretching mode at 3005 $cm^{-1}$, frequency differences are less than 1 $cm^{-1}$ between neat halothane and halothane in solution in hexadecane. Halothane in the hydrocarbon region of the phospholipid bilayer should have similar characteristics.

The most intense halothane Raman line at 714 $cm^{-1}$, assigned to the C–Br stretching mode (Thiemer & Nielson, 1957), is unsuitable for monitoring halothane concentrations in phospholipid dispersions since it overlaps the choline C–N stretching mode of the phospholipid at 717 $cm^{-1}$. The halothane band of next highest intensity appears at 310 $cm^{-1}$ and is assigned to the C–Br bending mode. Since this latter band is free of phospholipid spectral interference, we have used it to monitor the concentration of halothane.

Raman features due to halothane in the C–H and C–C stretching mode regions do not interfere appreciably with the phospholipid spectra in these spectral intervals. The 3005-$cm^{-1}$ band occurs above the C–H region of interest. Although halothane has a band in the 1128-$cm^{-1}$ region, this feature is quite weak and contributes negligible intensity at low halothane concentrations. At high halothane concentrations, the halothane contribution to the 1128-$cm^{-1}$ spectral intensity would be interpreted as making the hydrocarbon interior of the DPPC bilayers appear somewhat more ordered at a given temperature. A correction for such an effect has not been made.

*Concentration of Halothane.* Figure 2 presents the linear relationship that has been established between the mole ratio of halothane and DPPC ($n_{Hal}/n_{DPPC}$) and the spectral intensity ratio ($I_{Hal}/I_{DPPC}$) of the Raman bands of these substances. The DPPC C–C stretching mode feature at 1090 $cm^{-1}$ due to gauche bonds was selected for use, with the 310-$cm^{-1}$ band of halothane as being representative of phospholipid concentration. The peak height intensity ratio was measured at 45 °C, a temperature that is above the gel to liquid-crystal transition in pure DPPC dispersions. For most of the samples, the mole ratios were computed from the weights of pure halothane and 20% (w/w) DPPC dispersions. Above a mole ratio of 2.1, a separate halothane phase existed even at 45 °C. For very low mole ratios and for some other doubtful cases, the mole ratios were obtained indirectly from the measured $I_{Hal}/I_{DPPC}$ intensity ratios and the linear relationship in Figure 2.

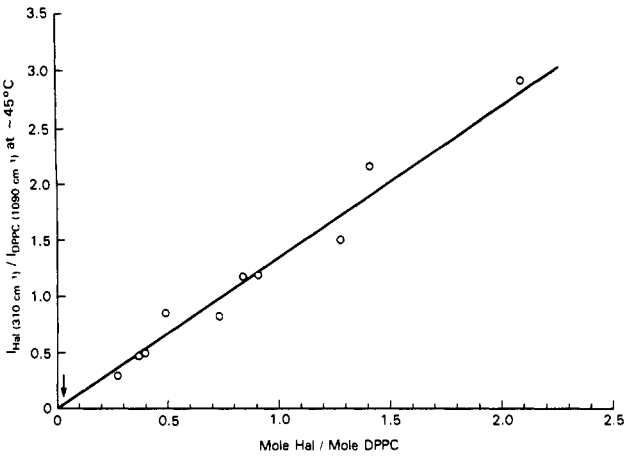


FIGURE 2: Linear relationship between the intensity ratio of the characteristic Raman bands and the mole ratio of halothane and DPPC. The arrow marks the dose level (1.3% in vapor phase) for general anesthesia.

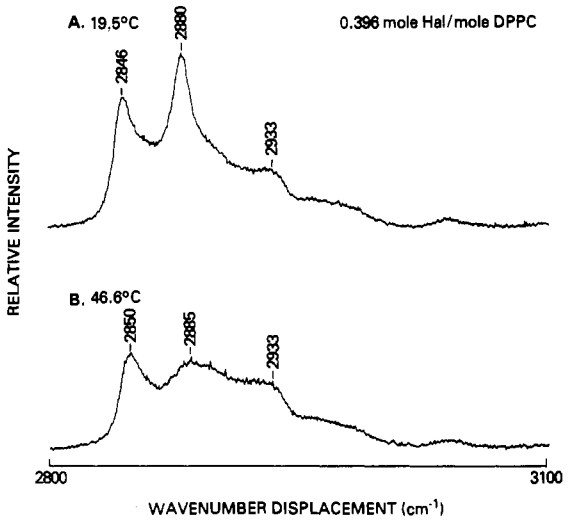


FIGURE 3: Raman spectra of the C–H stretching region of DPPC multilayers in the presence of halothane below and above the transition temperature. Each spectrum consists of a single scan.

*Effects of Halothane on the Thermal Transition of DPPC.* Figures 3 and 4 display representative Raman spectra of DPPC bilayers in the C–H and C–C stretching mode regions, respectively. They emphasize the well-known differences in these spectral intervals below and above the phase transition temperature (Levin, 1984; Bunow & Levin, 1977; Spiker & Levin, 1976). The gel to liquid-crystalline transformation was monitored by the $I_{2935}/I_{2880}$ peak height intensity ratios in the C–H stretching mode region and by the $I_{1090}/I_{1130}$ peak height ratio in the C–C stretching mode region. Plots of these two intensity ratios as a function of temperature are shown for a variety of $n_{Hal}/n_{DPPC}$ values in Figures 5 and 6. The bilayer transition temperature, $T_m$, decreases as halothane is added until a saturation limit is reached at a $n_{Hal}/n_{DPPC}$ value of about 1.25. Also, in the presence of halothane, the transition is broadened in comparison to that for pure DPPC multilayers dispersed in water. The transition breadth, however, is almost independent of the amount of halothane present. The limiting ratios in the low-temperature gel and high-temperature liquid-crystalline regions fall on essentially the same lines for all halothane concentrations. Some hysteresis was encountered in the transition curves when an ascending temperature experiment immediately followed a descending temperature one. We attribute this effect to slow equilibration in the static samples, especially when haloethane formed a separate phase

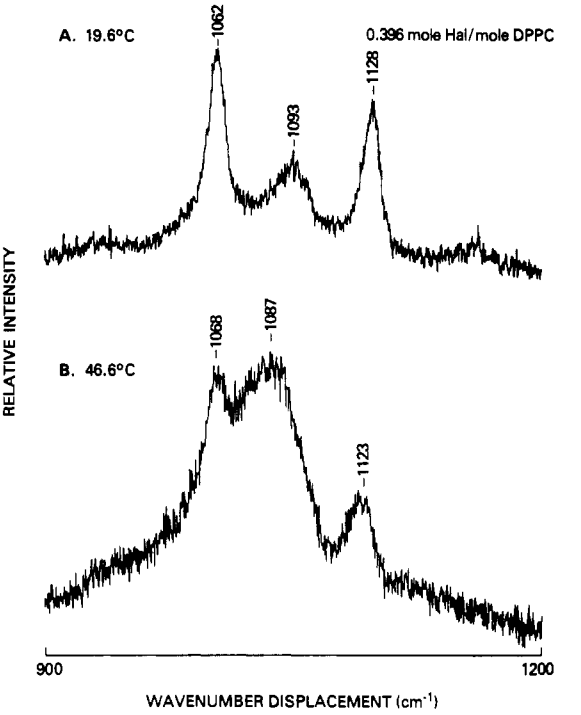


FIGURE 4: Raman spectra of the C–C stretching region of DPPC multilayers in the presence of halothane below and above the transition temperature. The top spectrum consists of two scans and the bottom five scans.

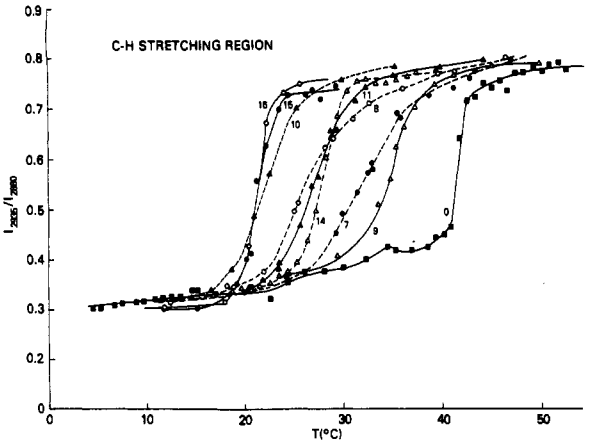


FIGURE 5: Thermal transition monitored in C–H stretching region. Run numbers on curves.

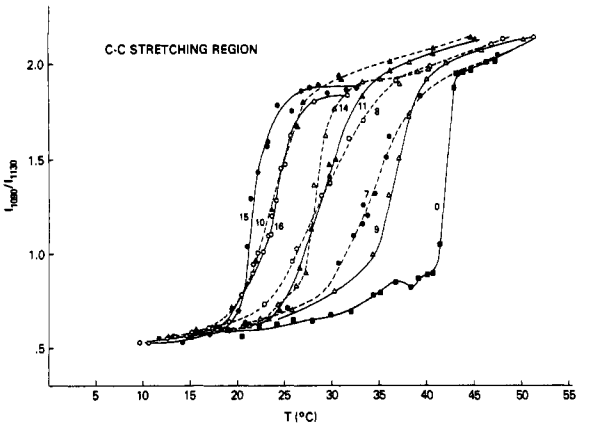


FIGURE 6: Thermal transition monitored in C–C stretching region. Run numbers on curves.

at lower temperatures and then only slowly diffused throughout the multiphase system. Some data in Figures 5 and 6 are from experiments in which the temperature was cycled up and down,

Table I: Transition Temperature as a Function of Halothane Content

| run | $n_{Hal}/n_{DPPC}$ from weights | $I_{Hal}/I_{DPPC}$ | $n_{Hal}/n_{DPPC}$ from Figure 2 | $T_m$ (°C) C–H | $T_m$ (°C) C–C | $-\Delta T_m$ (°C) C–H | $-\Delta T_m$ (°C) C–C |
|---|---|---|---|---|---|---|---|
| 0 | 0 | | | 41.4[a] | 42.0[a] | | |
| 2[b] | | 0.07 | 0.05 | 39.5 | 40.0 | 1.1 | 0.8 |
| 3[b] | | 0.17 | 0.13 | 38.2 | 39.0 | 2.4 | 1.8 |
| 4[b] | | 0.29 | 0.21 | 36.2 | 36.9 | 4.4 | 3.9 |
| 9[c] | 0.27 | 0.30 | 0.22 | 35.1 | 35.5 | 6.1 | 5.6 |
| 13 | 0.37 | 0.47 | | | | | |
| 6 | 0.48 | 0.85 | | | | | |
| 7[d] | 0.40 | 0.49 | 0.36 | 32.4 | 33.9 | 8.2 | 7.0 |
| 11[c] | 0.73 | 0.82 | 0.63 | 27.4 | 28.1 | 13.8 | 13.0 |
| 5[b] | | 1.17 | 0.94 | 26.2 | 27.6 | 14.4 | 13.2 |
| 14[e] | 0.84 | 1.16 | 0.87 | 27.8 | 28.3 | 13.6 | 13.7 |
| 8[d] | 0.91 | 1.19 | 0.88 | 25.8 | 28.1 | 14.8 | 12.8 |
| 10[c] | 1.28 | 1.50 | 1.11 | 22.6 | 23.1 | 18.6 | 18.0 |
| 15[e] | 1.41 | 2.15 | 1.60 | 21.4 | 21.8 | 20.0 | 20.2 |
| 16[e] | 2.08 | 2.89 | 2.15 | 21.2 | 24.2 | 20.2 | 17.8 |

[a] Maximum values from profiles of several samples. [b] For runs 2–5, $T_m^{CH}$ = 40.6 °C and $T_m^{CC}$ = 40.8 °C for 20% DPPC alone. [c] For runs 9–11, $T_m^{CH}$ = 41.2 °C and $T_m^{CC}$ = 41.1 °C for 20% DPPC alone. [d] For runs 7 and 8, $T_m^{CH}$ = 40.6 °C and $T_m^{CC}$ = 40.9 °C for 20% DPPC alone. [e] For runs 14–16, $T_m^{CH}$ = 41.4 °C and $T_m^{CC}$ = 42.0 °C for 20% DPPC alone.

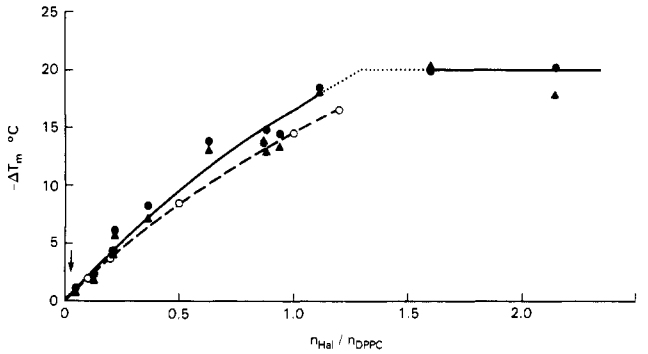


FIGURE 7: Depression in the transition temperature as a function of the ratio of moles of halothane to moles of DPPC. Experimental values: closed circles for C–H stretching region; closed triangles for C–C stretching region. Ideal solution theory: open circles and dashed line. $n_{Hal}/n_{DPPC}$ values derived from measured $I_{Hal}/I_{DPPC}$ values and graph (Figure 2 and Table I). The arrow marks the dose level (1.3% in vapor phase) for general anesthesia.

and other data are from experiments in which the temperature was only increased with reequilibration times of about 15 min at each new temperature.

Table I summarizes the data related to Figures 5 and 6. Runs 2–5, which are not shown graphically, were done before magnetic mixing was introduced and were run up and down the temperature range. Included in this table are $n_{Hal}/n_{DPPC}$ values derived directly from weighings and indirectly from $I_{Hal}/I_{DPPC}$ values. Also included in this table are the values of $T_m$, the transition temperatures for the various $n_{Hal}/n_{DPPC}$ values measured at the midpoint of the transition region, and the values of $-\Delta T_m$, the negative of the depression in the transition temperature compared to $T_m$ for pure DPPC multilayers. In general, the values of $-\Delta T_m$ reported by the C–C stretching region are somewhat smaller than the corresponding ones for the C–H stretching region. Figure 7 displays the relationship between $-\Delta T_m$ and $n_{Hal}/n_{DPPC}$ for observations in both the C–H stretching and C–C stretching mode regions. The dashed line through the open circle points in this figure gives $-\Delta T_m$ as derived from ideal solution theory. This calculation is discussed later.

*Distribution of Halothane between Phases.* At low $n_{Hal}/n_{DPPC}$ values, halothane distributes itself between three phases: the DPPC bilayers, water, and air. At high $n_{Hal}/n_{DPPC}$ values, a fourth phase of liquid halothane forms. Sufficient data are available in the literature to permit computation of the distribution of halothane between these phases on the basis of ideal (Henry's law) solution theory. In general, the results of these calculations concur with our experimental results and aid in the interpretation.

The calculation of the distribution of halothane between the phases can be formulated in terms of two equilibrium constant expressions, a volume ratio, and several mole ratios. The equilibrium constant expression for the distribution between the DPPC and water phases is written in terms of the mole fractions ($X$) of halothane in the two phases:

$$K_X = X_{Hal}(DPPC)/X_{Hal}(H_2O)$$

Because the concentration of halothane in the DPPC phase may be appreciable, it is not desirable to use a distribution expression defined in terms of molar concentrations. On the other hand, the equilibrium constant expression for the distribution of halothane between water and gas phases is conveniently written in molar concentrations. Thus

$$K_C = [Hal]_{H_2O}/[Hal]_{gas}$$

The volume ratio of the overall liquid and gas phases is

$$V_r = V_{gas}/V_{liq}$$

Two pairs of ratios of moles of material are defined. One pair consists simply of overall mole ratios:

$$R_1 = n_{Hal}/n_{DPPC}$$

and

$$R_2 = n_{H_2O}/n_{DPPC}$$

The other pair consists of ratios of moles of halothane in different phases:

$$\phi_1 = n_{Hal}(H_2O)/n_{Hal}(DPPC)$$

and

$$\phi_2 = n_{Hal}(gas)/n_{Hal}(DPPC)$$

With these definitions and the simplifying approximation that

$$X_{Hal}(H_2O) = n_{Hal}(H_2O)/n_{H_2O}$$

due to the low solubility of halothane in water, an overall expression for the distribution can be derived, namely:

$$\frac{K_X}{R_2} = \frac{1 + 1/\phi_1 + V_r/K_C}{R_1 + \phi_1 + V_r\phi_1/K_C + 1} \quad (1)$$

When the values for the distribution constants, $K_X$ and $K_C$, and the parameters, $V_r$, $R_1$, and $R_2$, are inserted, eq 1 can be

Table II: Equilibrium Constant for Distribution of Halothane between Water and Gas Phases and Related Quantities: $K_C = [Hal]_{H_2O}/[Hal]_{gas}$

| | temp (°C) | | | | | |
|---|---|---|---|---|---|---|
| | 20 | 25 | 30 | 35 | 40 | 45 |
| $K_C$[a] | 1.8 | 1.4 | 1.1 | 0.90 | 0.75 | [0.60][b] |
| $P_g$ (atm)[c] | 0.321 | 0.394 | 0.481 | 0.581 | 0.700 | 0.832 |
| $[Hal]^{satd}_{gas}$ (M) | 0.0133 | 0.0161 | 0.0193 | 0.0230 | 0.0272 | 0.0318 |
| $[Hal]^{satd}_{H_2O}$ (M)[a] | $0.024_0$ | $0.022_5$ | $0.021_2$ | $0.020_7$ | $0.020_4$ | $[0.019_1]$[b] |

[a] Data from Eger et al. (1965), Larson et al. (1962), Lowe and Hagler (1969), and Steward et al. (1973). [b] Values in brackets are extrapolations. [c] From Ohne (1976).

Table III: Distribution of Halothane between DPPC, Water, and Gas Phases[a]

| | $R_1$, $n_{Hal}/n_{DPPC}$ | $\phi_1$, $n_{Hal}(H_2O)/n_{Hal}(DPPC)$ | $\phi_2$, $n_{Hal}(gas)/n_{Hal}(DPPC)$ | $X_{Hal}(DPPC)$ | $X_{Hal}(H_2O) \times 10^3$ | $[Hal]_{DPPC}$ (mM) | $[Hal]_{H_2O}$ (mM) | $[Hal]_{gas}$ (mM) | % Hal saturation |
|---|---|---|---|---|---|---|---|---|---|
| LC[b] | 0.025 | 0.040 | 0.067 | 0.022 | 0.006 | 25 | 0.31[d] | 0.52 | 1.6 |
| Gel[c] | 0.025 | 0.145 | 0.081 | 0.020 | 0.018 | 22 | 1.01 | 0.56 | 4.2 |
| LC | 0.010 | 0.037 | 0.062 | 0.083 | 0.021 | 99 | 1.2 | 1.9 | 6.1 |
| Gel | 0.010 | 0.138 | 0.077 | 0.076 | 0.070 | 90 | 3.9 | 2.2 | 16 |
| LC | 0.50 | 0.028 | 0.047 | 0.32 | 0.080 | 510 | 4.4 | 7.4 | 23 |
| Gel | 0.50 | 0.104 | 0.058 | 0.30 | 0.275 | 470 | 15.3 | 8.5 | 64 |
| LC | 1.00 | 0.021 | 0.035 | 0.49 | 0.12 | 1000 | 6.8[d] | 11.4 | 36 |
| Gel[e] | 1.00 | *0.079* | *0.044* | *0.48* | *0.43* | *970* | *24* | *13* | *100* |
| LC | 2.1 | 0.014 | 0.023 | 0.67 | 0.17 | 2200 | 9.4[d] | 16 | 49 |
| Gel[e] | 2.1 | *0.079* | *0.044* | *0.48* | *0.43* | *970* | *24* | *13* | *100* |

[a] 20% (w/w) DPPC in water ($R_2 = n_{H_2O}/n_{DPPC} = 163$; $[DPPC]_{H_2O} = 0.34$ M); volume of gas phase equals volume of liquid phase ($V_r = 1$). [b] LC = liquid-crystalline phase at 45 °C. [c] Gel = gel phase at 20 °C. [d] Overall halothane concentration, considered to be in water only: for $\phi_1 = 2.1$, 716 mM. [e] A halothane phase exists. Values in italics are for saturation.

solved for $\phi_1$ by successive approximations in a computer program. As part of the same program, other quantities of interest can then be calculated as follows:

$$\phi_2 = V_r\phi_1/K_C$$

$$X_{Hal}(H_2O) = \frac{\phi_1 R_1}{R_2}\left(\frac{1}{\phi_1 + \phi_2 + 1}\right)$$

$$X_{Hal}(DPPC) = \frac{R_1}{R_1 + \phi_1 + \phi_2 + 1}$$

$$[Hal]_{DPPC} = \frac{(1.09\text{ M})X_{Hal}(DPPC)}{1 - X_{Hal}(DPPC)}$$

$$[Hal]_{H_2O} = \frac{(1000\text{ g/L})X_{Hal}(H_2O)}{18.0\text{ g/mol}}$$

$$[Hal]_{gas} = [Hal]_{H_2O}/K_C$$

and

$$\%\text{ Hal saturation} = 100[Hal]_{H_2O}/[Hal]^{satd}_{H_2O}$$

Data for calculating the distribution of halothane come from several sources. The $K_X$ distribution constant was found by Simon et al. (1979) to differ appreciably for the gel and liquid-crystalline forms of DPPC dispersion in 0.1 M aqueous sodium chloride solution. For the gel form (20–36 °C), $K_X = 1100$; for the liquid-crystalline form (41–55 °C), $K_X = 4000$. The latter value is in good agreement with the value of 3800 calculated from Hill's (1974) measurements of the depression in the transition temperature in a system without added salt. For our purposes, we assume that these distribution constants apply over the accessible concentration ranges in a nonsaline aqueous system. Table II gives selected literature values for the $K_C$ distribution constant and for the solubility of halothane in water at temperatures of interest. This table includes the vapor pressure ($P_g$) of neat halothane. The Bunsen coefficient, as employed by Smith et al. (1981), equals $K_C$ except for a $T/273$ K factor. This factor makes the $K_C$ values larger. With this adjustment, the agreement between the values for the Bunsen coefficients measured by these workers and the values for $K_C$ in Table II is satisfactory.

The solubility of halothane in water changes little over the temperature range of 20–40 °C. The corresponding decrease in $K_C$ is due almost entirely to the increase in vapor pressure of halothane. Because $K_C$ is not far from unity, the concentration of halothane in the gas phase is comparable to the concentration in the water phase.

Other values for the solubility of halothane in water have been reported. As part of an NMR study of the distribution of halothane between water and DPPC in dispersions, Koehler et al. (1977) state that "...amounts of halothane greater than $4.7 \times 10^{-2}$ M exceed the solubility of halothane in water..." presumably at 25 °C. This exceptionally high value is undoubtedly a consequence of overlooking the presence of a significant amount of the halothane resident in the gas volume in the 10-mm NMR tube. Using the accepted solubility value of $2.2 \times 10^{-2}$ M from Table II and the reported value of $4.7 \times 10^{-2}$ M, we estimate that the gas volume in the NMR tube was about 1.5 times the water volume, which is reasonable for the experiment. This example illustrates the importance of taking account of the gas volume in analyzing the distribution of an inhalation anesthetic such as halothane, especially when the phospholipid/water ratio is low. The example also shows that it is essential to work with sealed sample containers and to guard against loss of volatile anesthetics in preparing samples. This problem was noted by Koehler et al. (1978) in a subsequent paper.

Table III presents the results of calculations of the distribution of halothane between the three phases over the range of conditions of the present experiments. For all of our experiments, the concentration of DPPC was 20% (w/w), which fixes the ratio $R_2$ at 163. The volume of the gas phase was taken as equal to the volume of the overall liquid phase even though this volume ratio was not carefully controlled in the present experiments. A second set of calculations with $V_r =$

Table IV: Conditions for a Clinically Active Level of Halothane in DPPC at 45 °C[a]

| | | | | $V_r = 0$[b] | | $V_r = 1$[b] | |
|---|---|---|---|---|---|---|---|
| % DPPC (w/w) | $R_2$, $n_{H_2O}/n_{DPPC}$ | $X_{Hal}$(DPPC) | $[Hal]_{H_2O}$ (mM) | $R_1$, $n_{Hal}/n_{DPPC}$ | $[Hal]^{all}_{H_2O}$ (mM) | $R_1$, $n_{Hal}/n_{DPPC}$ | $[Hal]^{all}_{H_2O}$ (mM) |
| 20 | 163 | 0.021 | 0.30 | 0.023 | 7.8 | 0.025 | 8.5 |
| 10 | 367 | 0.021 | 0.30 | 0.024 | 3.6 | 0.027 | 4.1 |
| 1 | 4040 | 0.021 | 0.30 | 0.044 | 0.60 | 0.080 | 1.1 |
| 0.1 | 40700 | 0.021 | 0.30 | 0.24 | 0.33 | 0.60 | 0.82 |
| 0.01 | 408000 | 0.021 | 0.30 | 2.2 | 0.30 | 6.0 | 0.82 |

[a] Partial pressure of halothane = 0.013 atm. [b] $V_r$ = volume of gas phase/volume of liquid phase.

0 showed little sensitivity to $V_r$, an outcome which is a consequence of using the rather high value of $R_2$. The calculations were done in pairs: one for the gel state (Gel) at 20 °C; one for the liquid-crystalline state (LC) at 45 °C. The entries in Table III range from the physiologically active level at $R_1$ = 0.025 at the top of the table to near-saturation in the DPPC gel state at $R_1$ = 1.0 (calculated) to saturation in the DPPC liquid-crystalline state at $R_1$ = 2.1 (observed). As can be seen by comparing the values in the columns headed $[Hal]_{DPPC}$, $[Hal]_{H_2O}$, and $[Hal]_{gas}$, the concentration in the DPPC phase is much higher than in the other two phases, except when the halothane phase separates out at high $R_1$ values. In all cases, the mole fraction of halothane in the DPPC phase, $X_{Hal}$(DPPC), changes little in going through the phase transition despite the change by a factor of nearly 4 in $K_X$. Only relatively small amounts of the halothane in the DPPC phase need be transferred to the water (and gas) phases, even though the concentration in the water phase changes by more than a factor of 3. The concentration in the gas phase changes little during the transition due to compensatory changes in $K_C$ and $K_X$. For comparable volumes of the water and gas phases, these two phases hold comparable amounts of halothane. For comparison with the manner in which some other experiments have been reported and for use below, a footnote to Table III gives the *overall* concentration of halothane considered to be in water only.

To obtain an estimate of the halothane environment that the Raman experiment samples, we should consider the concentration of halothane *in DPPC viewed as dispersed in water* in comparison with the concentration of the anesthetic in the water phase. A simple comparison of $[Hal]_{DPPC}$ and $[Hal]_{H_2O}$, concentrations of halothane in the separate phases, is insufficient. To obtain such an *effective* halothane concentration, $[Hal]^{eff}_{DPPC}$, in a well-mixed dispersion with $V_r = 1$, we subtract $[Hal]_{H_2O}$ and $[Hal]_{gas}$ from the *overall* halothane concentration viewed as dispersed in water only. (This overall concentration is expressed as $[Hal]^{all}_{H_2O}$ below.) For $R_1$ = 0.025, this overall halothane concentration is 8.5 mM; for $R_1$ = 1.0, it is 341 mM (footnote *d* of Table III). As a consequence, we have values of $[Hal]^{eff}_{DPPC}$ of 7.7 mM (LC) and 6.9 mM (gel) for the first case and of 323 mM (LC) and 305 mM (Gel) for the other case. These give $[Hal]^{eff}_{DPPC}/[Hal]_{H_2O}$ ratios of 7 or greater in the various combinations. In our experiments in which the laser beam sampled the compacted multilayer part of the sample, the $[Hal]^{eff}_{DPPC}/[Hal]_{H_2O}$ ratios were even larger. Thus, the observation of the 310-$cm^{-1}$ band of halothane is representative of halothane predominantly in the DPPC phase under all of the present experimental conditions.

*Clinical Levels of Halothane.* Clinical concentrations of halothane in the inhaled gas are variously reported between 0.75% (Mountcastle et al., 1978) and 1.3% (Mastrangelo et al., 1978; Simon et al., 1979) at 37 °C. For the lowest concentration entry at $n_{Hal}/n_{DPPC}$ = 0.025 in Table III, the equilibrium halothane concentration in the gas phase is essentially 1.3% for both the liquid-crystalline and gel phases. The concentration in DPPC is about 0.02 mole fraction or 0.6% (w/w). Arrows in Figures 2 and 7 mark the 1.3% dose level. Our lowest concentration experiment was conducted with $n_{Hal}/n_{DPPC}$ = 0.05, which gave a depression of 1.1 °C in the transition temperature. Extrapolation of the experimental data in Figure 7 shows that the depression in the transition temperature under the clinical conditions is about 0.5 °C. In addition to causing an observable lowering in the transition temperature, the clinical concentration of halothane would also cause an observable broadening of the phase transition region.

Various concentrations of phospholipid have been used in published studies of the effect of halothane on the fluidity of phospholipid multilayers (Ueda et al., 1986; Rosenberg, 1980). Consequently, we have employed our distribution expressions to explore the varying conditions for the clinically active level of halothane partial pressure. Table IV shows the results of these calculations for two assumptions about the size of the gas volume: (1) negligible gas volume ($V_r$ = 0); (2) equal gas- and liquid-phase volumes ($V_r$ = 1). This table gives the relationship between the concentration of DPPC and the *overall* concentration of halothane considered to be in water only, $[Hal]^{all}_{H_2O}$ as well as related mole ratios. We have used $[Hal]^{all}_{H_2O}$ because that is how the concentration of halothane is expressed in many published reports. Of course, Table IV shows that the concentrations of halothane in the DPPC phase, $X_{Hal}$(DPPC) and in the water phase, $[Hal]H_2O$, are fixed when the concentration in the gas phase is fixed. The necessary values of $[Hal]^{all}_{H_2O}$ decrease as the concentration of DPPC decreases until a limiting value of $[Hal]^{all}_{H_2O}$ is reached at about 0.1% DPPC. This limiting relationship was found experimentally by Vanderkooi et al. (1977). They saw no change in the thermotropic transition curve for the closely related system of dimyristoylphosphatidylcholine (DMPC)/halothane as the DMPC composition was increased from 0.01% to 0.3%. Comparing results for the two assumptions about the volume of the gas phase, we see that the necessary value of $[Hal]^{all}_{H_2O}$ is strongly dependent on the concentration of phospholipid in the low concentration range. Expressed another way, the concentrations, $X_{Hal}$(DPPC) and $[Hal]_{H_2O}$, are strongly dependent on the relative volume of the gas and liquid phases as well as on $[Hal]^{all}_{H_2O}$ at low phospholipid concentrations. Thus, uncertainties about gas volumes for experiments conducted under low phospholipid concentrations place the results of such experiments in doubt. On the other hand, Table IV assures us that the present experiments done with high phospholipid concentrations are weakly dependent on the relative volumes of gas and liquid phases.

*Thermodynamics of Halothane/DPPC Mixtures.* Hill (1974) and Vanderkooi et al. (1977) have applied ideal solution theory to the depression of the transition temperature in phospholipid dispersions due to anesthetics. In its simplest form, ideal solution theory excludes the solute from the solid phase of the solvent. Thus, to apply the corresponding thermodynamic expression to the present experiments, we assume that for the gel state the halothane molecules are excluded from the lipid region of the phospholipid bilayer that undergoes the disordering monitored by our Raman experiments. The

overall concentration of halothane in the DPPC, however, does not change appreciably (Table III). We shall return to this point below. The appropriate thermodynamic relationship between the mole fraction of the DPPC "solvent" ($X_{DPPC}$) and the transition temperature is the van't Hoff equation:

$$\ln X_{DPPC} = \frac{-\Delta H^\circ}{R}\left(\frac{1}{T} - \frac{1}{T_0}\right) \quad (2)$$

where $\Delta H^\circ$ = 8.76 kcal/mol (Albon & Sturtevant, 1978) and $T_0$ = 314.6 K. With values of $X_{DPPC} = 1 - X_{Hal}$(DPPC) derived for the liquid-crystalline form as in Table III, values for $-\Delta T_m$, the depressions in $T_m$, were calculated from eq 2. These $-\Delta T_m$ values are plotted vs. $n_{Hal}/n_{DPPC}$ values in Figure 7. The fairly good agreement between the simple ideal solution theory and the present experiments in the subsaturation regime is gratifying.

Although the line in Figure 7 calculated from ideal solution theory is reasonably independent of the concentration of DPPC ($n_{H_2O}/n_{DPPC}$) and the size of the gas volume in the regime of our experiments, this line is not universally applicable. As the entries in Table IV imply, systems with low DPPC concentrations and different gas volumes have quite different $n_{Hal}/n_{DPPC}$ values for a given mole fraction of halothane in the DPPC phase.

A limiting depression of the transition temperature of about 21 °C was observed for an $n_{Hal}/n_{DPPC}$ value of about 1.25. Also, as seen in Figures 5 and 6, the transition region steepens again under these limiting conditions. The results of the distribution calculations given in Table III concur with the observation of this limiting effect. For an $n_{Hal}/n_{DPPC}$ value of about 1.0, the degree of halothane saturation in the water phase in equilibrium with the gel state at 20 °C was calculated to be 100%. Thus, at $n_{Hal}/n_{DPPC}$ ratios about this value, one expects a halothane phase to separate when the gel state is formed. Experimentally, above an $n_{Hal}/n_{DPPC}$ value of 2.1, a halothane phase coexists with the liquid-crystalline form as well. Of course, the simple ideal solution expression does not account for saturation effects in this regime.

## Discussion

*Effect of Halothane at the Clinical Level.* Our vibrational Raman spectroscopic experiments show a small but measurable depression in the transition temperature and broadening of the transition region when halothane is present at the clinically active level in DPPC dispersions. The arrow in Figure 7 points to an $n_{Hal}/n_{DPPC}$ value of 0.025, the clinical level in the present experiments, which gives a $\Delta T_m$ of −0.5 °C. The evidence for this small value is reinforced by the overall $-\Delta T_m$ vs. $n_{Hal}/n_{DPPC}$ curve as determined by measurements at higher halothane concentrations. The good agreement through much of the concentration range between ideal solution theory, as represented by the dashed line in Figure 7, and our observations provides further support for this conclusion.

A measurable effect of halothane at the clinically active level has been found with several other experimental methods. These observations include microcalorimetry (Mountcastle et al., 1978), turbidimetry (Kamaya et al., 1979; Hill, 1974), and electron spin resonance (ESR) (Trudell et al., 1973; Mastrangelo et al., 1978). The spin-label ESR experiments were done with phospholipids that contained cholesterol. As was noted in the last part under Results, the effective $n_{Hal}/n_{DPPC}$ value may vary substantially with experimental conditions. However, $\Delta T_m$ should not change since its value is fixed by the equality of the chemical potential between the gas phase, the water phase, and the DPPC phase. For the present experiments, $n_{Hal}/n_{DPPC}$ for the clinical level is rather insensitive to small changes in the DPPC concentraton and in the volume of the gas phase.

For the microcalorimetry experiments (Mountcastle et al., 1978), in which the halothane concentration was controlled by its partial pressure of 0.014 atm in the gas phase, the concentration of DPPC was 1%. Assuming a negligible gas volume, we compute $n_{Hal}/n_{DPPC}$ = 0.044 (Table IV). A $\Delta T_m$ of −0.45 °C was observed.

For the turbidimetric experiments of Kamaya et al. (1979), in which the halothane concentration was also controlled by its partial pressure of 0.01 atm, the concentration of DPPC was not given. However, $\Delta T_m$ = −0.6 °C for the clinical concentration, as read from a graph. From Hill's reduced data (Hill, 1974), for his turbidimetric measurements with 0.04% DPPC, we compute $\Delta T_m$ = −0.5 °C and $n_{Hal}/n_{DPPC}$ = 1.5, assuming equal gas and liquid volumes.

In the spin-label experiments of Mastrangelo et al. (1978), a change of 1.3% in the order parameter was observed at the clinical level of halothane in egg yolk phosphatidylcholine containing 21% (w/w) cholesterol. These workers used 1.3% halothane in the gas phase to control the concentration of halothane in solution at 20 °C. The concentration of phospholipid was 8%, and $n_{Hal}/n_{DPPC}$ was reported as 0.030 for this system in which the solubility of halothane in the lipid is about twice as great as in pure DPPC in the gel phase at the same temperature.

In contrast to the foregoing observations of observable effects of clinical levels of halothane is the report of no observable effect under these conditions by Lieb et al. (1982). They studied dimyristoylphosphatidylcholine–cholesterol dispersions by the Raman method. One would not expect the change from egg yolk PC in the previously cited ESR experiment (Mastrangelo et al., 1978) to DMPC in the presence of added cholesterol to be determinative. Their samples contained about 3% DMPC to which 40 mol % cholesterol had been added. Halothane solutions were prepared and handled by syringe techniques, and equilibrium concentrations of halothane in water were calculated from a distribution coefficient that was about 4 times smaller than comparable published ones for cholesterol-containing systems (Simon et al., 1979; Mastrangelo et al., 1978; Smith et al., 1981). Also, the gas volume in the sample capillaries was not taken into account. Consequently, there is good reason to suppose that the solutions studied were less concentrated in halothane than reported, which could contribute to a failure to observe an effect at the supposed clinical level.

On the other hand, it is possible that the effect is too small to observe by the Raman method in cholesterol-containing systems. Our experiments (Figures 5 and 6) show that once the fully liquid-crystalline region is reached the same degree of bilayer disorder is found for DPPC dispersions containing different amounts of halothane. Under these conditions, the effect of added halothane would not be discernible. The effect of adding cholesterol to the phospholipid is to broaden the transition region and increase the order in the liquid-crystalline state (Levin, 1984). Hence, it is understandable that the effect of halothane at the clinical level might be unobservable by Raman spectroscopy of DMPC–cholesterol systems.

As we and others have used Raman spectroscopy, only the changes induced by the anesthetic on the fluidity of the hydrocarbon interior of the phospholipid have been monitored. Circumstantial evidence going back to the celebrated Meyer–Overton correlation between anesthetic potency and solubility in olive oil supported the idea that anesthetic action was

a consequence of change only in the hydrocarbon interior. Increasingly, investigators are questioning this interpretation and suggesting a role for the phospholipid head group, if, alternatively, the mechanism of anesthesia is not a more direct effect on membrane proteins.

*Implications of the Temperature Profiles.* We now turn to several aspects of the interaction of halothane with DPPC bilayers that emerge from a consideration of the full set of transition curves, Figures 5 and 6, and the graph of $-\Delta T_m$ vs. $n_{Hal}/n_{DPPC}$ in Figure 7.

Halothane has a marked effect at low concentrations on the pretransition that is observed for pure DPPC dispersions in the vicinity of 36 °C. The pretransition was not observed even at the lowest halothane concentration in the present experiments using $I_{2935}/I_{2880}$ and $I_{1090}/I_{1130}$ indexes. In the microcalorimetry experiments of Mountcastle et al. (1978) in which the pretransition was seen prominently for pure DPPC dispersions, this feature was appreciably broadened and shifted to a lower temperature at the clinical level of halothane concentration, which is half the lowest concentration studied directly in the present experiments. At approximately 3 times the clinical level of halothane, these workers observed no pretransition.

As will be argued more fully below, the halothane molecules are located only in the head-group region when the DPPC liposomes are in the gel state. Since small concentrations of halothane have a marked effect on the pretransition, it seems likely that halothane head-group perturbation affects the acyl chain lattice reorganizations governing the pretransition.

In Figures 5 and 6, it is apparent that the amplitude of the overall transition is essentially unchanged by successive additions of halothane. For the low-temperature, gel-state end, curves for all halothane concentrations ultimately join the pure DPPC curve. Similarly, in the high-temperature, liquid-crystalline region, all curves come close to the disorder reached by pure DPPC. We take this constancy of amplitude to imply that the *thermal* entropy of the transition of the hydrocarbon interior of the phospholipid bilayers is little changed by the addition of halothane (Huang et al., 1982). *Thermal* entropy is that part of the entropy that is due to the distributions over molecular energy states such as internal rotational levels. To a first approximation, thermal entropy in this system is separable from the entropy contribution due to spatial mixing which appears to be nearly ideal. This interpretation is supported in Figure 7 by the reasonable fit through much of the concentration range between the experimental values of $-\Delta T_m$ and the dashed line calculated from ideal solution theory. The increases in entropy in the bilayer associated with successively lower $T_m$ values are due largely to an increase in entropy of mixing.

In the temperature profiles in Figures 5 and 6, some increase in the transition breadth is found. However, this effect does not increase in proportion to the amount of halothane added. The irregularities seen in the slopes of some of the curves in the transition region we attribute to difficulties in achieving halothane redistribution after halothane phase separation occurs at low temperatures. The decrease in slope that does occur in the transition region implies a decrease in the cooperative unit size for DPPC molecules during the melting phenomenon.

Saturation by halothane occurs in the phospholipid bilayers in two ways. In the liquid-crystalline regime, halothane saturation was observed at an $n_{Hal}/n_{DPPC}$ value of about 2.1. As shown in Table III, the distribution calculation gives the corresponding mole fraction of halothane in the DPPC as about 0.67 but a degree of saturation of only 50%. Evidently, the ideal solution treatment for the DPPC bilayers fails rather abruptly at an $n_{Hal}/n_{DPPC}$ value of about 1.5, as seen in Figure 7. For the gel state, the distribution calculations, as summarized in Table III, show that saturation should occur at a halothane mole fraction of about 0.5 in the DPPC phase. Thus, as the $n_{Hal}/n_{DPPC}$ value rises from about 1.25 and 2.1, increasing amounts of halothane must be driven out of the bilayer as the temperature of the system drops during a transition. This limiting process is reflected in the increasing steepness of the transition curves until a nearly vertical slope is reached at 21 °C.

The two different, near-integer values of the halothane concentration in the phospholipid bilayer for the two conditions of saturation are strongly suggestive. For the gel phase, the saturation ratio of molecules of halothane to molecules of DPPC is approximately 1:1. Space-filling molecular models of the Kendrew type (Ealing) of DPPC and halothane show that each DPPC molecule in the all-trans hydrocarbon conformation has room only in the head-group region and only for one of the rather large halothane molecules. In modeling the DPPC molecule, no attempt was made to include hydrating water molecules. For the liquid-crystalline state, the saturation ratio of halothane to DPPC is about 2:1. The models show that a second halothane molecule can be accommodated in the fluidized hydrocarbon region, provided that the halothane molecule is not too close to the ester end of the fatty acid chains, but, that is all. To make room for an additional halothane molecule would require a substantial input of Gibbs free energy in order to expand the bilayer structure. Forming the pure liquid halothane phase is preferable. At halothane mole fractions that are less than the gel-regime saturation value of $X_{Hal}(DPPC) \approx 0.5$, while relatively little halothane leaves the phospholipid phase during a decreasing temperature transition (Table III), halothane molecules do move out of the hydrocarbon interior into the head-group region. This exclusion of halothane molecules from the hydrocarbon region during gel formation is in keeping with the good fit of the experimental data to simple ideal solution theory.

At first thought, the two $n_{Hal}/n_{DPPC}$ saturation values of about 1:1 and 2:1 seem to be in conflict with the two distribution coefficients for the gel and liquid-crystalline regimes. For the gel phase, $K_X = 1100$; for the liquid-crystalline phase, $K_X = 4000$. These values were measured for $n_{Hal}/n_{DPPC}$ values well removed from saturation. Under these conditions, the molecular models suggest that approximately three *possible*, distinct sites exist for a halothane molecule within the space occupied by each pair of hydrocarbon chains. However, when one such site is occupied in association with the hydrocarbon chains of a single DPPC molecule, the other sites are no longer available. Thus, at low concentrations, the ratio of halothane sites in the liquid-crystalline phase to halothane sites in the gel phase is about 4 to 1, but at higher concentrations, saturation is reached at a ratio of about 2 to 1.

In Table I, a persistent difference is found between the transition temperatures monitored in the C–C and C–H stretching regions. In all experiments, paired C–C and C–H measurements were made at each temperature, thereby reinforcing the evidence for a systematic difference. The $T_m$'s monitored in the C–H region are lower. Since changes in this region are understood to reflect changes in *inter*chain interactions with perhaps some superposition of trans/gauche isomerizations (Gaber et al., 1978; Huang et al., 1982), it appears that the hydrocarbon chain lattice first expands somewhat before rotations around C–C bonds become excited.

*Halothane/DPPC Head-Group Interactions.* In the remaining discussion, we consider evidence for an important role for the phospholipid head-group region. First, as discussed above, the effect of a clinical level of halothane on the hydrocarbon interior even of pure DPPC bilayers is small. When cholesterol is present in a truer model of the matrix of a cell membrane, the effect on the hydrocarbon interior is muted and perhaps unobservable. Second, as emphasized by Lieb et al. (1982), the small effect of halothane and similar anesthetics on the hydrocarbon interior can be largely reversed by a small temperature change, one which is insufficient to affect anesthesia in living systems. Third, consideration of the results of distribution calculations displayed in Table III showed that the concentration of halothane changed very little in the DPPC phase *as a whole* during the transition from the gel to the liquid-crystalline state. Yet, the good fit of $\Delta T_m$'s computed from ideal solution theory implies that halothane is being "frozen out" of the hydrocarbon interior. Thus, the halothane was displaced into the head-group region. Despite the rather polar character of the head-group region, it must be receptive to halothane, which, after all, has some polarity and a weakly acidic hydrogen.

A fourth and rather direct line of evidence for a significant presence of halothane in the head-group region comes from various NMR experiments. Shieh et al. (1975, 1976) studied the effect of halothane on line widths of the proton signals from DPPC in sonicated dispersions. They also observed changes in the chemical shift of the halothane proton. They found that narrowing of the peak due to $CH_3$ protons of the choline moiety of the head group occurred in the gel region as halothane was introduced near room temperature. At higher concentrations of halothane, the peaks due to the protons of the palmitoyl chains also narrowed, and the chemical shift of the halothane proton moved upfield as is characteristic of a less polar environment. These observations are consistent with halothane molecules first entering the head-group region in the gel state and then inducing the formation of liquid-crystalline-state clusters at higher halothane concentrations.

Koehler et al. (1978, 1980) employed $^{19}F$, $^{13}C$, and $^{31}P$ NMR to investigate the microenvironments of halothane in DPPC dispersions. From changes in chemical shifts and line widths in the $^{19}F$ NMR spectra, these investigators identified two or possibly three sites for halothane molecules in the phospholipid bilayer. Halothane molecules in the head-group region had essentially the same chemical shift as in the water phase, but the HF splitting was gone, which implies less mobility for the halothane molecules in the head-group region than in water. At 25 °C, much higher concentrations of halothane introduce a broad, higher field signal due to molecules that penetrate the partly melted hydrocarbon interior, where rotational motion of the halothane molecules is restricted. The change in chemical shift is consistent with a fraction of the halothane molecules residing in the nonpolar hydrocarbon environment. Changes in $^{13}C$ signals from the choline carbon and $^{31}P$ signals from the phosphate groups narrowed in response to additions of halothane. This evidence further supports the interpretation that halothane molecules reside in the head-group region and significantly increase head-group mobility.

## Conclusions

Through the intensity of the 310-$cm^{-1}$ C–Br bending mode of halothane, $CF_3CBrCl_H$, Raman spectroscopy provides a direct measure of the concentration of this anesthetic in aqueous DPPC dispersions. This measurement strengthens the usefulness of Raman spectroscopy for studying the influence of halothane on the order/disorder characteristics of the hydrocarbon interior of DPPC bilayers as reflected in the intensity changes in the C–H and C–C stretching regions.

Temperature profiles of the gel to liquid-crystal phase transition show a marked influence of halothane. The transition temperature decreases from 41.5 °C for pure DPPC to 21 °C for saturation with halothane in this model membrane system.

Systematic distribution calculations have been applied to the aqueous halothane/DPPC system and have aided the interpretation of the experiments. The results of these calculations have underlined the importance of taking account of the gas volume that is accessible to volative anesthetics such as halothane. Often in the literature, only the overall concentration of the anesthetic in solution is reported. However, the concentration of the anesthetic in the phospholipid phase, which determines the effect on the transition temperature, is dependent both on the concentration of the phospholipid and on the gas volume accessible to the anesthetic. In studies of the effect of a volatile anesthetic at the dilute, clinical level, it is essential that the concentrations be controlled and well-known. For the present study, the use of 20% DPPC aqueous dispersions caused most of the halothane to be in the phospholipid phase, thereby simplifying the system.

Over much of the range of halothane concentrations, experimental values of $\Delta T_m$, the change in the transition temperature, are consistent with ones calculated from simple ideal solution theory. It is understood that halothane molecules are excluded from the "frozen" or gel phase hydrocarbon interior of the bilayers. However, halothane molecules remain in the head-group region in the gel state up to a saturation value of about one halothane molecule per DPPC molecule. In the liquid-crystalline phase, saturation corresponds to about two halothane molecules per DPPC molecule.

The present data and several reports in the literature indicate an observable $\Delta T_m$ of about −0.5 °C at the low clinical level of halothane. However, apparently conflicting studies report no observable effect, especially when cholesterol is a significant component of the bilayers. Uncertainties about the control of the halothane concentrations cast doubt on these negative findings.

Both indirect evidence from the partitioning data in the present experiments and more direct evidence from published NMR studies indicate that the significant interaction between halothane and the bilayer matrix occurs in the phospholipid head-group region. Although the effect of halothane on the structural and dynamic properties of the bilayer is small for clinical concentrations, the perturbations are consistent with the hypotheses relating anesthetic properties to phospholipid-mediated effects (Lechleiter et al., 1986).

## Acknowledgments

N.C.C. is grateful to the National Institutes of Health for support of his contributions to this investigation.

## References

Albon, N., & Sturtevant, J. M. (1978) *Biochemistry 17*, 2258–2260.

Bunow, M. R., & Levin, I. W. (1977) *Biochim. Biophys. Acta 487*, 388–394.

Craig, N. C., & Levin, I. W. (1979) *Appl. Spectrosc. 33*, 475–476.

Eger, E. I., II, Saidman, L. J., & Brandstater, B. (1965) *Anesthesiology 26*, 764–770.

Gaber, B. P., Yager, P., & Peticolas, W. L. (1978) *Biophys. J. 21*, 161–176.

Hill, M. W. (1974) *Biochim. Biophys. Acta 356*, 117-124.
Huang, C. H., Lapides, J. R., & Levin, I. W. (1982) *J. Am. Chem. Soc. 22*, 5926-5930.
Janoff, A. S., & Miller, K. W. (1982) in *Biological Membranes* (Chapman, D., Ed.) pp 417-476, Academic Press, New York.
Janoff, A. S., Pringle, M. J., & Miller, K. W. (1981) *Biochim. Biophys. Acta 649*, 121-128.
Kamaya, H., Ueda, I., Moore, P. S., & Eyring, H. (1979) *Biochim. Biophys. Acta 550*, 131-137.
Koehler, K. A., Jain, M. K., Stone, E. E., Fossel, E. T., & Koehler, L. S. (1978) *Biochim. Biophys. Acta 510*, 177-185.
Koehler, L. S., Fossel, E. T., & Koehler, K. A. (1977) *Biochemistry 16*, 3700-3706.
Koehler, L. S., Fossel, E. T., & Kohler, K. A. (1980) *Prog. Anesthesiol. 2*, 447-455.
Larson, C. P., Jr., Eger, E. I., II, & Severinghaus, J. W. (1962) *Anesthesiology 23*, 349-355.
Lechleiter, J., Wells, M., & Gruener, R. (1986) *Biochim. Biophys. Acta 856*, 640-645.
Levin, I. W. (1984) *Adv. Infrared Raman Spectrosc. 11*, 1-48.
Lieb, W. R., Kovalycsik, M., & Mendelsohn, R. (1982) *Biochim. Biophys. Acta 688*, 388-398.
Lippert, J. L., & Peticolas, W. L. (1971) *Proc. Natl. Acad. Sci. U.S.A. 68*, 1572-1576.
Lowe, H. J., & Hagler, K. (1969) in *Gas Chromatography in Biology and Medicine* (Porter, R., Ed.) pp 86-112, Churchill, London.
Mastrangelo, C. J., Trudell, J. R., Edmunds, H. N., & Cohen, E. N. (1978) *Mol. Pharmacol. 14*, 463-467.
Mountcastle, D. B., Biltonen, B. L., & Halsey, M. J. (1978) *Proc. Natl. Acad. Sci. U.S.A. 75*, 4906-4910.
Ohne, S. (1976) *Computer-Aided Data Book for Vapor Pressure*, p 175, Data Book Publishing Co., Tokyo.
O'Leary, T. J., Ross, P. D., & Levin, I. W. (1984) *Biochemistry 23*, 4636-4641.
Rosenberg, P. H. (1980) *Prog. Anesthesiol.* 325-334.
Rosenberg, P. H. Eibl, H., & Stier, A. (1975) *Mol. Pharmacol. 11*, 879-882.
Roth, S. H. (1979) *Annu. Rev. Pharmacol. Toxicol. 19*, 159-178.
Shieh, D. D., Ueda, I., & Eyring, H. (1975) *Prog. Anesthesiol. 1*, 307-312.
Shieh, D. D., Ueda, I., Lin, H.-C., & Eyring, H. (1976) *Proc. Natl. Acad. Sci. U.S.A. 73*, 3999-4002.
Simon, S. A., McIntosh, T. J., Bennett, P. B., & Shrivastav, B. B. (1979) *Mol. Pharmacol. 16*, 163-170.
Smith, R. A., Porter, E. G., & Miller, K. W. (1981) *Biochim. Biophys. Acta 645*, 327-338.
Spiker, R. C., Jr., & Levin, I. W. (1976) *Biochim. Biophys. Acta 455*, 560-575.
Steward, A., Allott, P. R., Cowles, A. L., & Mapleson, W. W. (1973) *Br. J. Anaesth. 45*, 282-293.
Thiemer, R., & Nielson, J. R. (1957) *J. Chem. Phys. 27*, 887-890.
Trudell, J. R., Hubbell, W. L., & Cohen, E. N. (1973) *Biochim. Biophys. Acta 291*, 321-327.
Ueda, I., & Kamaya, H. (1984) *Anesth., Analg., Reanim. 63*, 929-945.
Ueda, I., Hirakawa, M., Arakawa, K., & Kamaya, H. (1986) *Anesthesiology 64*, 67-71.
Vanderkooi, J. M., Landesberg, R., Selick, H. I., & McDonald, G. G. (1977) *Biochim. Biophys. Acta 464*, 1-16.
Wong, P. T. T. (1984) *Annu. Rev. Biophys. Bioeng. 13*, 1-24.

# Spin Trapping of Precursors of Thymine Damage in X-Irradiated DNA†

Mikinori Kuwabara,* Osamu Inanami, Daiji Endoh, and Fumiaki Sato
*Department of Radiation Biology, Faculty of Veterinary Medicine, Hokkaido University, Sapporo 060, Japan*
*Received September 9, 1986; Revised Manuscript Received December 24, 1986*

ABSTRACT: A spin-trapping method combined with ESR spectroscopy was utilized to obtain evidence for the presence of precursor radicals leading to damage in X-irradiated DNA. Two technical improvements were introduced to the conventional spin-trapping method to make possible its application to large molecules such as DNA: (1) prior to X irradiation, sonolysis of aqueous DNA solution by 19.5-kHz ultrasound was made to get a highly concentrated DNA solution and to lower the viscosity of the solution; (2) after precursor radicals in X-irradiated DNA were trapped by a spin-trapping reagent, the DNA was digested to oligonucleotides by DNase I to get an ESR spectrum with a well-resolved hyperfine structure. Thus, it was recognized that the ESR spectrum obtained after X irradiation of the aqueous solution containing DNA and the nitroso spin-trapping reagent 2-methyl-2-nitrosopropane consisted of at least three sets of signals in the DNA. Identification of free radicals was made by comparing the spectrum with that of thymidine, which was precisely examined by a spin-trapping method combining two kinds of spin traps (nitroso and nitrone compounds) with liquid chromatography. As a result, all the signals were identified as the spin adducts of radicals produced at the thymine base moiety of DNA. The 5-hydroxy-5,6-dihydrothymin-6-yl radical was identified as a precursor of 5,6-dihydroxy-5,6-dihydrothymine (thymine glycol), the 6-hydroxy-5,6-dihydrothymin-5-yl radical as a precursor of 6-hydroxy-5,6-dihydrothymine, and the 5-methyleneuracil radical as a precursor of 5-(hydroxymethyl)uracil.

OH radicals are generated via arachidonic acid metabolism in platelets, leukocytes, macrophages, hemangioendothelial cells, and microsomes, as well as in electron transport systems in mitochondria. They are regarded as potential inducers of cellular activity and tissue responses such as inflammation (Kuehl & Egan, 1980; Murota, 1984), whereas ionizing radiation is well-known to be the most convenient tool for gen-

† This is work performed at Hokkaido University under contract with the Power Reactor and Nuclear Fuel Development Corp.

0006-2960/87/0426-2458$01.50/0 © 1987 American Chemical Society